Infrared Spectroscopy of Carbo-Cations upon Electron Ionization of Ethylene in Helium Nanodroplets

Swetha Erukala¹, Alexandra Feinberg¹, Amandeep Singh¹ and Andrey F. Vilesov^{1,2,*}

¹ Department of Chemistry, University of Southern California, Los Angeles, California 90089, USA

² Department of Physics and Astronomy, University of Southern California, Los Angeles, California 90089, USA

Abstract

Electron impact ionization of helium droplets doped with ethylene molecules and clusters yields

diverse C_XH_Y⁺ cations embedded in the droplets. The ionization primarily produces C₂H₂⁺, C₂H₃⁺,

C₂H₄⁺ and CH₂⁺, whereas larger carbocations are produced upon reactions of the primary ions with

ethylene molecules. Vibrational excitation of the cations leads to the release of bare cations and

cations with a few helium atoms attached. Laser excitation spectra of the embedded cations show

well resolved vibrational bands with a few wavenumber widths - an order of magnitude less than

previously obtained in solid matrices or molecular beams by tagging techniques. Comparison with

previous studies of free and tagged CH₂⁺, CH₃⁺, C₂H₂⁺, C₂H₃⁺ and C₂H₄⁺ cations shows that the

helium matrix typically introduces a shift in vibrational frequencies of less than about 20 cm⁻¹,

enabling direct comparisons with the results of quantum chemical calculations for structure

determination. This work demonstrates a facile technique for production and spectroscopic study

of diverse carbocations, which act as important intermediates in gas and condensed phases.

*Author to whom correspondence should be addressed.

Electronic address: vilesov@usc.edu.

1

1. Introduction

Molecular cations are important intermediates in the chemistry of condensed phases or in the gas phase such as in earth's upper atmosphere or outer space.¹⁻⁴ In comparison to neutrals, cations remain much less studied. Information on their structure mainly come from NMR studies.⁵ The structure of many rather simple cations such as CH₄⁺ ⁶, ⁷, CH₅⁺ ⁸⁻¹⁰, C₄H₇⁺ ¹¹⁻¹³ etc. is still debated. Cation structure can be implied from characteristic vibrational frequencies and infrared intensities upon comparison with theoretical results from quantum chemical calculations. 14-16 Because of the low density, only absorption spectra of small cations, such as CH₂⁺, ¹⁷ CH₃⁺, ¹⁸ C₂H₂⁺, ¹⁹C₂H₃^{+ 20} etc. were obtained in the gas phase. The study of larger cations usually involves action spectroscopy in molecular beams. The ions of interest are tagged with Ar atoms or hydrogen molecules while their absorption is tracked by dissociation of the complexes.²¹⁻²⁴ Tagging methods, however, may cause the complexes to exhibit band splitting due to lowering of symmetry or the presence of isomers. The interpretation of the spectra of the complexes can also require extensive quantum chemical calculations. Recently introduced cooling techniques in cryogenic traps filled with helium gas has enabled lowering the temperature of the cations to $\sim 5\mbox{--}10~\mbox{K}$ and tagging with the most weakly bound helium atoms. 21, 25, 26 Experiments in cryogenic traps were also used to obtain the spectra of free (untagged) ions such as CH5⁺¹⁰ and C3H2⁺²⁷ by monitoring faster reactivity of vibrationally excited ions.

Isolation in solid matrices composed of argon, neon and H_2 presents another opportunity to ion spectroscopy. Although solid matrices have been used extensively for absorption spectroscopy of molecules and radicals, their use for ions is more involved due to the small concentration of ions, large background signal from neutral precursors, and lack of mass resolution. Isolation in liquid helium droplets is a natural extension of this approach. Liquid helium is the ultimate spectroscopic matrix for a variety of reasons: its low temperature of ~ 0.4 K, superfluid state and related homogeneous environment, weak interaction with dopants, and high ionization potential (24.6 eV). For about 3 decades, spectroscopy in helium droplets has been used extensively to study molecules and molecular clusters. However, ion spectroscopy made its mark in the last decade after Drabbels *et al.* 8 showed that that ions could be produced in helium droplets via photoionization. Another important experiment was that of von Helden *et al.* 9 who showed that ions originating from an electrospray could be captured by helium droplets. It was

also obtained that the embedded ions could be set free upon irradiation with resonant infrared radiation, providing a convenient monitor of the absorption. Nevertheless, employing photoionization or electrospray techniques require a more involved apparatus compared to a typical helium droplet spectroscopic setup and actually imposes limitations on the kind of ions that can be studied. Electron impact ionization presents a viable alternative. It's well known that electron impact ionization of helium droplets doped with neutral species leads to the production of molecular ions and ionic fragments. A few percent of those produced can be decorated with several helium atoms, enabling a variant of the tagging experiments. For example, Scheier *et al.*, showed that the electron impact ionization of C_{60} in helium droplets leads to the formation of C_{60} clusters with $n \leq 100$. Ellis *et al.* recently produced complexes of protonated acetic acid and protonated carbon dioxide tagged with a few helium atoms C_{60} and reported their infrared spectra. We have shown that embedded C_{60} and C_{60} and C_{60} in helium atoms can be obtained upon electron impact ionization of embedded C_{60} and C_{60} in the complex ionization of embedded C_{60} and C_{60} in the complex ionization of embedded C_{60} in the complex ionization in the complex ionization of embedded C_{60} in the complex ionization in the

In this work, we show that a variety of embedded $C_XH_Y^+$ cations can be produced upon electron impact ionization of ethylene-doped helium droplets. Absorption of multiple infrared photons leads to release of bare cations as well as their clusters with a few attached helium atoms. Infrared spectra of the cations in the CH-stretching range show narrow vibrational bands with a few wavenumber widths, which is an order of magnitude less than previously obtained in solid matrices or in tagged complexes. Comparison with previous studies of some small free cations shows that the helium matrix introduces a shift in vibrational frequencies of about or less than ± 20 cm⁻¹, which enables direct comparisons with the results of quantum chemical calculations. This work demonstrates the utility of a straightforward electron impact ionization technique for production and spectroscopic study of carbocations embedded in helium droplets which could be expanded using the appropriate neutral precursors.

2. Experimental

Figure 1 shows the schematic of the experimental apparatus used for measuring infrared spectra of ions in helium droplets which has been described previously. 46 Helium droplet pulses of $\sim 250 \,\mu s$ width are produced upon expansion of helium gas at stagnation pressure of $P_0 = 20 \, bar$ and temperature of $T_0 = 23$ K in vacuum through a 1 mm diameter pulsed nozzle (General Valve series 99) attached to a Sumitomo RDK 408 refrigerator. 48 At these conditions, the droplets have average size of ~7000 He atoms. 46 Upon collimation by a 2 mm diameter skimmer, He droplets enter the 44 cm long pickup chamber where they capture ethylene molecules. Ethylene backfills the entire vacuum chamber. Its pressure is regulated by a leak valve and measured by an ionization pressure gauge. Further downstream, doped droplets pass through a differential pumping stage and enter the detection chamber that hosts a quadrupole mass spectrometer (QMS) (Extrel MAX 500) with an additional axial external ionizer placed ~ 20 cm upstream from the ionizer of the QMS, which will be referred to as probe ionizer. In standard QMS operation, doped droplets are ionized by electron impact in the probe ionizer. During the spectroscopic experiments reported in this work the droplets are ionized with the external ionizer set to 100 eV, 10 mA. Upon ionization, heavy droplet-ion moieties continue traversing towards the ion range of the probe ionizer, whereas light moieties are rejected by Einzel lenses which acts as a high pass filter.

Doped ionic droplets are irradiated by a focused infrared laser beam when they pass through the ion range of the probe ionizer. Absorption of several infrared quanta leads to production of free ions, which are then extracted, mass selected by the QMS and detected by an MCP.⁴⁶ The signal from the QMS is amplified and measured by a SR250 boxcar integrator with an appropriate gate and delay with respect to the laser pulse to account for the time of flight of the ions through the QMS. For measurements of the IR spectra with QMS fixed to a particular mass the gate was set to $\sim 10~\mu s$. This work employed an unseeded pulsed optical parametric oscillator-amplifier (Laser Vision, spectral resolution: $\sim 1~cm^{-1}$, pulse duration $\sim 7~ns$, pulse energy ~ 5 - 8 mJ, repetition rate 20 Hz). The absolute frequency of the laser is calibrated using the photo-acoustic spectrum of methane and ammonia molecules.

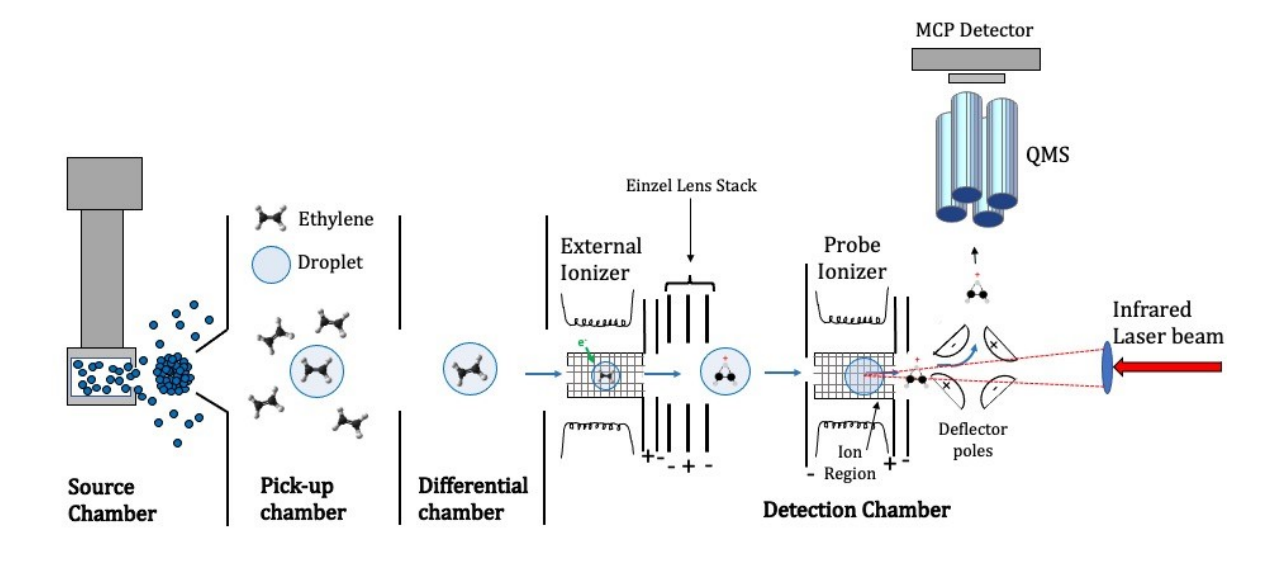


Figure 1. Schematic of the helium droplet setup. Helium droplets are produced from a cold pulsed nozzle in the source chamber. The droplets capture dopants in the pickup chamber and traverse into the detection chamber equipped with two electron impact ionizers: external and probe. The droplets are ionized in the external ionizer and interact with the counter propagating infrared laser beam once in the ion region of the probe ionizer. The released ions are mass selected by the quadrupole mass spectrometer.

3. Results

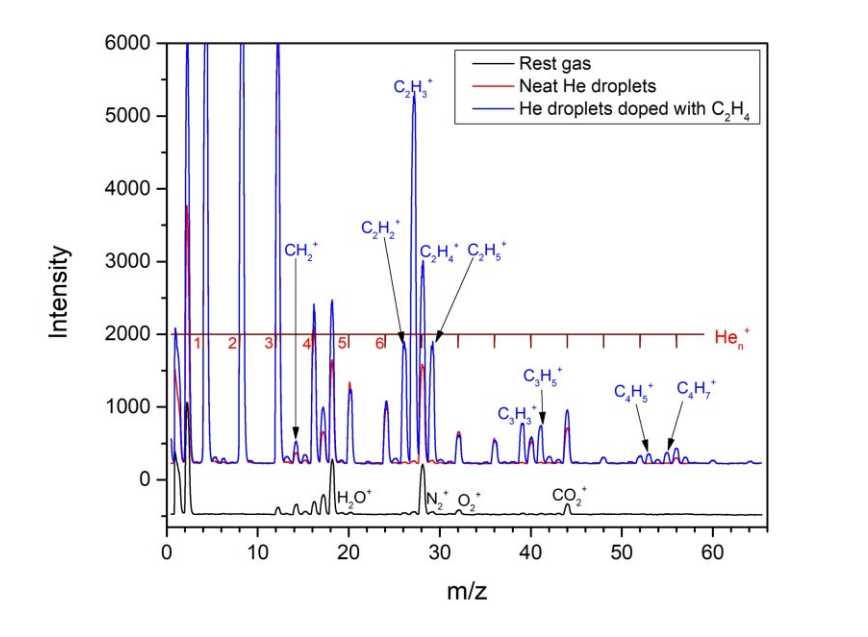


Figure 2. Mass spectra obtained with the probe ionizer. Black trace - baseline due to residual gas in the detection chamber. Red trace - neat helium droplets. Blue trace - helium droplets dopped at 4.5×10^{-6} mbar of ethylene. The traces are plotted to the same scale.

Figure 2 shows the mass spectra of the helium droplets upon standard ionization in the probe ionizer . The intensity was recorded around the maxima of the droplet pulses within the gate of 150 μ s. The gate was delayed by ~3.07 ms with respect to the trigger of the pulsed valve to account for the time of flight of the droplets in the vacuum apparatus. The black trace shows the base signal with the gate valve (between the pumping stage and the detection chamber) closed and a residual pressure in the detection chamber of ~ 5×10^{-9} mbar. The peaks correspond to the H⁺, H_2^+ $H_2^ H_2^+$ $H_2^ H_2^+$ and H_2^+ ions and some other weaker peaks from residual gases. The red trace shows the mass spectrum upon ionization of the neat helium droplet beam. It contains a sequence of H_2^+ peaks that exhibit decreasing intensity with H_2^+ it is seen that with the helium droplet beam, the intensity of the residual gas peaks of H_2^- and H_2^- and H_2^- increases. We assign this effect to ionization of water molecules in the residual gas by H_2^+ and H_2^- , which are produced upon the electron impact. Peaks due to H_2^- and H_2^- overlap with H_2^- and H_2^- , respectively. Due to low

residual gas pressure along the helium droplet beam path of $\sim 10^{-9}$ mbar, this additional signal at masses of OH⁺, H₂O⁺, N₂⁺ and CO₂⁺ cannot stem from the impurities captured by the droplets. Blue trace shows the mass spectrum with 4.5×10^{-6} mbar of ethylene in the pickup chamber. New intense peaks in the spectrum correspond to C₂H₂⁺, C₂H₃⁺ and C₂H₅⁺. The comparison of red and blue traces also shows that the ionization of the doped droplets yields CH₂⁺, C₂H₄⁺, C₃H₃⁺, C₃H₅⁺, C₄H₅⁺, C₄H₇⁺ as well as some other less abundant ions.

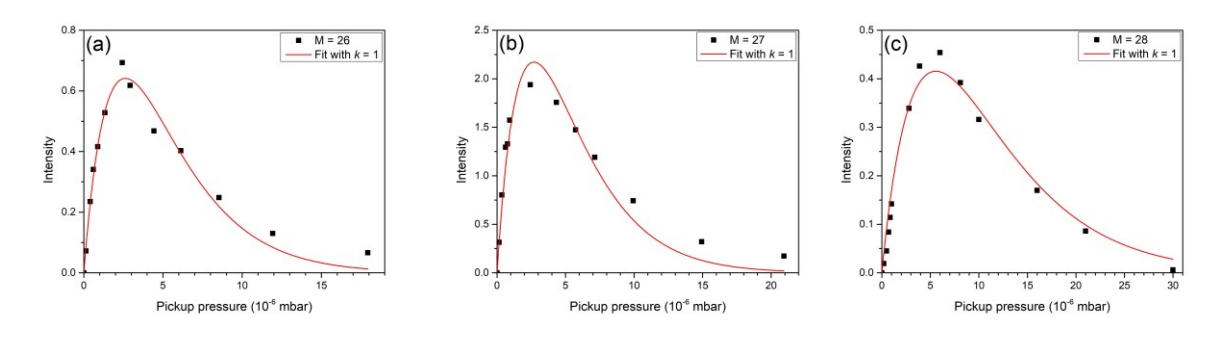


Figure 3. Ethylene pickup pressure dependence of the signal at M=26, M=27 and M=28 is shown by black squares. In c) the baseline signal due to He_7^+ and N_2^+ at zero ethylene pressure was subtracted. Red curves are fits with Poison dependence for pickup of single molecule.

Figure 3 shows the dependence of the intensity of the $C_2H_2^+$ (a) $C_2H_3^+$ (b) and $C_2H_4^+$ (c) peaks in the mass spectrum versus ethylene pressure, P, in the pickup chamber. Here (and later) the given pressure corresponds to the ion gauge reading. The absolute pressure could be obtained by dividing the reading by the sensitivity coefficient for ethylene of 2.3. The curves are fits of the data points by Poisson probability:

$$I_k(P) = C \cdot \frac{(P/A)^k}{k!} e^{-P/A} \tag{1}$$

for capture of k- ethylene molecules per droplet, with A and C fitting parameters. At P = A, on average one molecule is captured per droplet with $I_1(P=A)$ being the maximum. It is seen that fits with k=1 provide a good representation of the data points. At small pressure, the intensity rises linearly, consistent with pickup of single molecules. For both $C_2H_2^+$ and $C_2H_3^+$, the maxima at 2.7 ×10⁻⁶ mbar corresponds to the pickup pressure at which the droplets are doped with a single

ethylene molecule on average. This indicates that the free $C_2H_2^+$ and $C_2H_3^+$ cations are predominantly produced upon the ionization of droplets containing single ethylene molecules. An overshoot of the data points at $P > 10^{-5}$ mbar indicates that some minor yield of the ions are from ethylene clusters. In comparison, the dependence for $C_2H_4^+$ has maximum at 5.6×10^{-6} mbar, which corresponds approximately to two captured ethylene molecules per droplet. Nevertheless, the initial rise is still linear and the Poisson dependence with k=1 gives a good fit. This discrepancy most likely indicates that the $C_2H_4^+$ ions are produced from single embedded ethylene molecules as well as from small clusters, such as dimers and trimers.

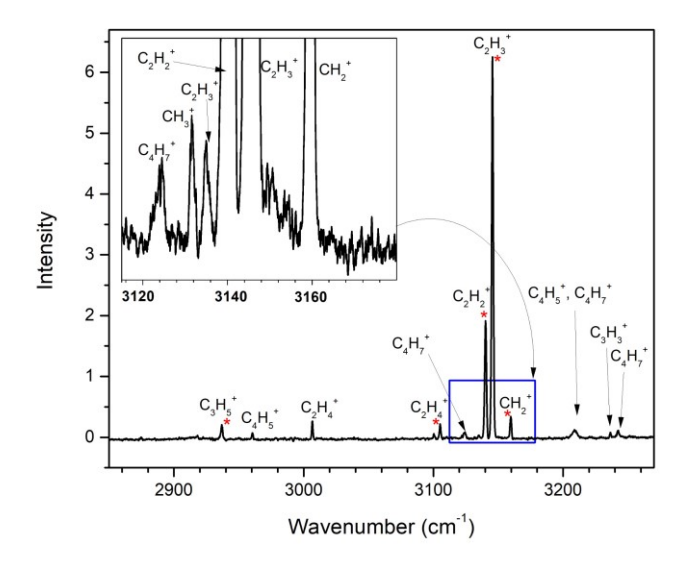


Figure 4. The total yield of ions upon laser irradiation of the ethylene doped ionized droplets. The insert shows an additional scan in the indicated range recorded with about a factor of \sim 10 higher amplification. The assignment of the spectral peaks is indicated.

Figure 4 shows the spectrum of the total ion yield upon laser irradiation of droplets doped with ethylene (4×10⁻⁶ mbar) and that were ionized in the external ionizer with the probe ionizer off. During the measurements, the DC of the QMS was off so that all ions produced upon laser irradiation were guided to the detector independent of their mass. The boxcar gate was set to 150 µs to accept ions with different masses which have different time of flight through the QMS. The main trace was obtained at low amplification to avoid saturation of the most intense peaks. The trace in the insert was recorded separately with a factor of ~10 larger amplification to discern weak

peaks. Figure 4 shows that the full ion spectrum has large number of peaks assigned to different ions as it will be explained in the following. It is seen that the most intense peaks correspond to $C_2H_2^+$ and $C_2H_3^+$ ions which are also most prominent in the mass spectrum in Fig. 2.

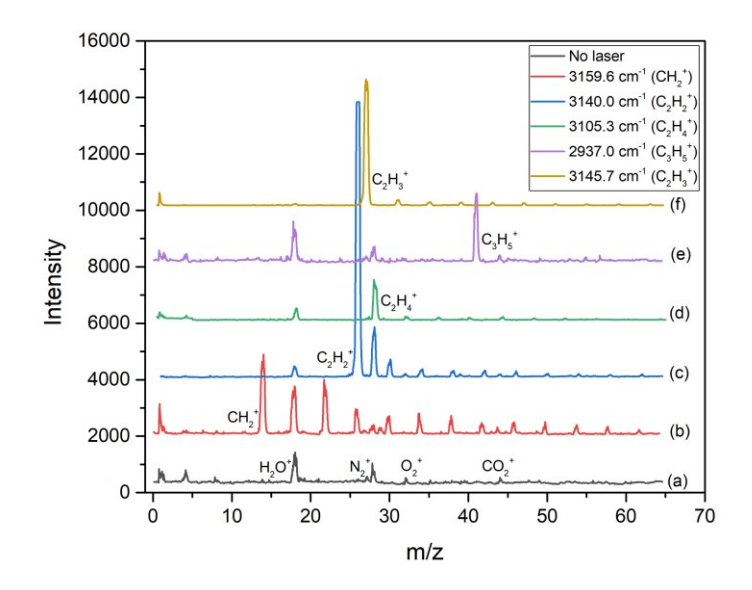


Figure 5. Mass spectra measured with laser parked at the spectral peaks as indicated in the legend. Trace a) was obtained with laser blocked.

For the assignment of the peaks in Fig. 4, the laser frequency was set to the maximum of a spectral peak and the mass spectrum was recorded with the boxcar gate of 150 μs. Fig. 5 (b-f) shows examples for CH₂⁺, C₂H₂⁺, C₂H₃⁺, C₂H₄⁺ and C₃H₅⁺ as indicated in the legend. The corresponding lines are marked by asterisks in Fig. 4. Trace a) shows the baseline mass spectrum recorded with the laser beam blocked and contains some weak peaks due to H₂O⁺, N₂⁺, O₂⁺ and CO₂⁺. The ions are likely produced from the residual gas ionization within the ion range of the probe ionizer upon encounters with metastable He* atoms which are produced in the external ionizer. In comparison, traces b)-e) show some new features. Trace b) recorded upon laser excitation at 3159.6 cm⁻¹ has a strong peak at M=14 au, and a sequence of peaks at higher masses with increments of 4 au and decreasing intensity. These peaks are assigned to free CH₂⁺ ions and CH₂⁺He_N clusters. Thus, the spectral peak at 3159.6 cm⁻¹ belongs to CH₂⁺ in helium droplets. In the mass spectra, the lowest mass of the laser induced peak gives the parent ion in helium droplets. Accordingly traces c)-e) correspond to the excitation of C₂H₂⁺, C₂H₄⁺, C₃H₅⁺ and C₂H₃⁺ ions in

helium droplets, respectively. Similarly, the other spectral peaks in Fig. 4 were assigned to different ions. The appearance of the M^+He_N peaks depends on the type of ion and the propensity towards the release of the M^+He_N clusters which seems to be weaker for larger ions, so that the $C_3H_5^+He_N$ peaks are not discernable. Trace c) is unusual in that besides M=26 which is due to $C_2H_2^+$ ions, it contains a sizable additional peak at M=28 and some weak progression of the corresponding helium cluster peaks. It is feasible that M=28 signal comes from weakly bound complexes $C_2H_2^+$ with H_2 molecules in helium droplets which has close frequency with $C_2H_2^+$.

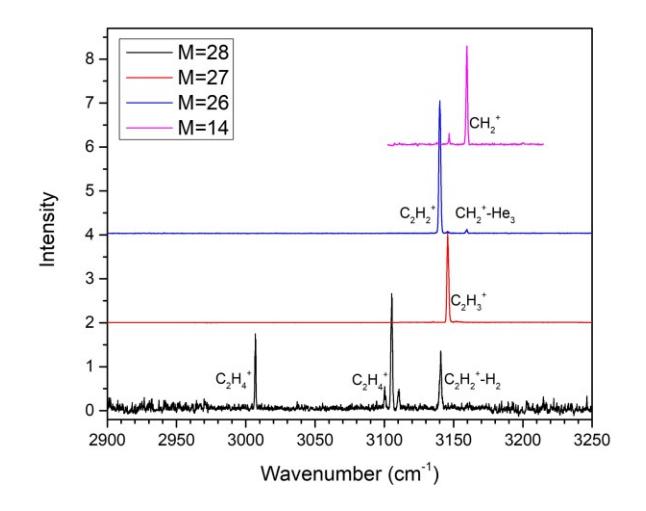


Figure 6. Spectra recorded at M=14 (pink), 26 (blue), 27 (red) and 28 (black).

Figure 6 shows the infrared spectra measured with the QMS fixed at M=14 (pink), 26 (blue), 27 (red) and 28 (black). No other bands were observed in broader range from 2600 to 3300 cm⁻¹. The spectrum of CH₂⁺ has an intense peak at 3159.6 cm⁻¹ and a weak peak at 3146.9 cm⁻¹ which will be further discussed in Section 4.5. The prominent peak in the blue trace at 3140.0 cm⁻¹ is due to acetylene cations, C₂H₂⁺ which has a single C-H infrared active band. The weak peak in the blue trace at 3159.5 cm⁻¹ is assigned to CH₂⁺ in helium droplets that contributes to measurements at M=26 via CH₂⁺-He₃ complexes. The two peaks in the black trace at 3007.0 and 3105.3 cm⁻¹ belong to ethylene cations, C₂H₄⁺. Similar to ethylene, ethylene cations are expected to have two infrared active C-H stretching bands. ^{30,31,50} The higher frequency v₉ band is a *b*-type transition due to the in-phase asymmetric stretch of the two CH₂ groups. The v₉ band of C₂H₄⁺ appears as a triplet which is assigned to the partially resolved rotational structure of the perpendicular band, similar to that observed for CH₃⁺ in helium. ⁴⁷ The third intense peak at 3140.8 cm⁻¹ may not be assigned to C₂H₄⁺ which must only have two C-H infrared active bands. The

position of the peak is very close and about 0.8 cm^{-1} shifted with respect to the 3140.0 cm^{-1} peak of $C_2H_2^+$. Therefore, we tentatively assigned this peak to $C_2H_2^+$ - H_2 complexes as it is obtained with QMS tuned to M=28. The spectrum of $C_2H_3^+$ (red trace) has a single, strong peak consistent with bridged structure of the complex. $^{20, 51}$ The bands assigned to CH_2^+ , $C_2H_2^+$ and $C_2H_3^+$ in Fig. 6 have frequencies close to the corresponding bands of free ions. $^{17, 19, 20, 52}$

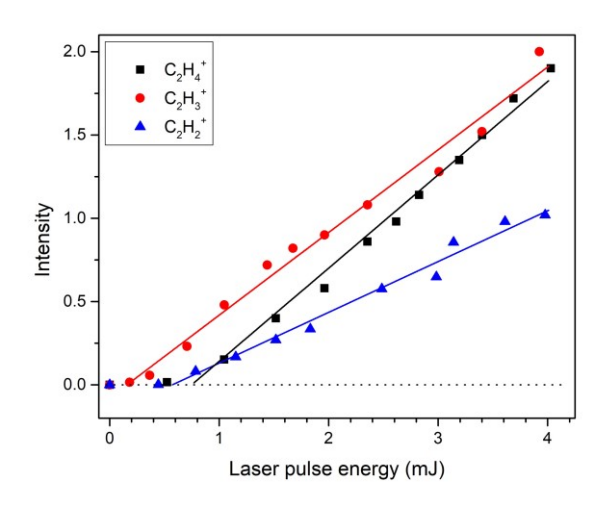


Figure 7. Laser pulse energy dependence of the signal for $C_2H_2^+$ at 3140.0 cm⁻¹ (blue), $C_2H_3^+$ at 3145.7 cm⁻¹ (red) and $C_2H_4^+$ at 3105.3 cm⁻¹ (black).

Figure 7 shows the laser pulse energy dependence of the $C_2H_2^+$, $C_2H_3^+$ and $C_2H_4^+$ bands in Fig. 6. The laser pulsed energy is measured at the entrance to the vacuum apparatus. For the shown bands, the signal is very low at the laser pulse energy of less than ~ 0.5 mJ and then rises approximately linear at >1 mJ. Similar laser pulse energy dependencies with an onset threshold were observed previously for $H_5O_2^{+46}$ and CH_3^{+47} in helium droplets, consistent with the absorption of multiple photons required for producing free ions. The onset threshold energy is approximately proportional to the band width divided by infrared intensity of the transition. However the values of the onset in this work and in Ref. should not be compared due to the realignment of the focusing lens between the measurements. The spectra reported in this work were measured at the maximum available laser pulse energy of ~ 4 mJ/pulse.

Figure 8 shows the dependence of the intensity of the $C_2H_2^+$ (a), and $C_2H_3^+$ (b) and $C_2H_4^+$ (c) bands versus the ethylene pressure in the pickup chamber. The curves are fits to Poisson distributions for the capture of k molecules per droplet. It is seen that for both $C_2H_2^+$ (a), and $C_2H_3^+$ (b), the intensities rise linearly at small pressures and have maxima at 3.0×10^{-6} mbar and 3.3×10^{-6}

mbar, respectively, somewhat higher as compared to that observed for free cations in Fig. 3. In comparison, the $C_2H_4^+$ signal has an initial quadratic rise vs pressure, has a maximum at $5.2 \times 10^-$ mbar and is well fit with the Poisson dependence for k=2. This indicates that the production of embedded $C_2H_4^+$ cations predominantly involve the ionization of droplets containing ethylene dimers. The quality of the fit for $C_2H_2^+$ (a) and $C_2H_3^+$ (b) with k=1 is worse than that in Fig. 3 a), b). In particular, the observed dependence has a smaller width than the Poisson fit. The origin of

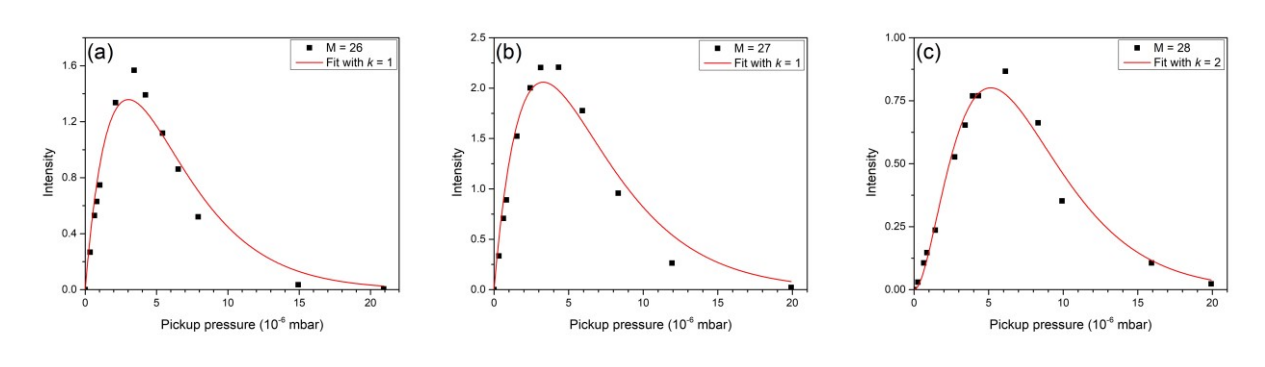


Figure 8. Ethylene pickup pressure dependencies of the laser induced signal for $C_2H_2^+$ at 3139.8 cm⁻¹, $C_2H_3^+$ at 3144.4 cm⁻¹ and $C_2H_4^+$ at 3105.3 cm⁻¹ as measured at M=26 (a) M=27 (b) and M=28 (c), respectively. Curves are fits of the data points by Poisson probability for capture of k molecules per droplet.

this effect remains to be explained. Commonly, the fit undershoots the experimental data at high pressures which is exemplified in Fig. 3. Note that using the Poisson probability function is an approximation because of the droplet size distribution, changing droplet cross section as well as scattering of the beam upon the pickup of the dopants. In this work, the scattering effect will be amplified by the deflection of charged droplets which occurs due to the electric field between the external ionizer and the ion range of the probe ionizer. Previous works with neutral dopants indicated that the experimental dependencies deviate from Poisson fits with integer *k*-values, especially at high pressure. If the signal contains contributions from different number of the captured molecules it is difficult to quantify the contributions from different number of the captured particles. In this situation, the power of the dependence at small pickup pressures and the position of the maxima usually serves as a good estimate for the number of the embedded species.

The spectroscopic experiment on ions in helium droplets could be further improved. Results such as in Fig. 4 call for replacing the quadrupole mass spectrometer as used in this work by a time-of-flight mass spectrometer. This will enable simultaneous measurements of the spectra

for all the embedded ions in a single laser scan. The nonlinear energy dependence of the laser pulse observed in this work and previously in Refs.^{40, 46} is inconvenient and may complicate the identification of weak bands. This effect relates to the absorption of multiple infrared photons required for evaporation of the entire droplet. Possible improvement of the technique may involve production of ions in larger droplets followed by subsequent moderation of the droplet size, which could be achieved upon multiple collisions with helium atoms at room temperature in an RF ion guide, as recently demonstrated by Scheier *et al.*⁵³

4. Discussion

This work confirms earlier observations^{46, 47} that electron impact ionization of helium droplets doped with molecules leads to the production of both free as well as embedded ions. Doping with ethylene molecules yields a variety of $C_XH_Y^+$ cations. The most abundant free and embedded fragments are splitter ions such as CH_2^+ , $C_2H_2^+$, $C_2H_3^+$ and $C_2H_4^+$ Observation of weaker signals from ions such as $C_3H_5^+$ and $C_4H_5^+$ shows that ionization of ethylene dimers can yield larger embedded cations containing three or four carbon atoms resulting from ion-molecule reactions. Resonant laser excitation of the embedded species causes the release of free cations which may have several attached helium atoms. Infrared spectra are obtained by monitoring the intensity of specific released ions. All observed C-H bands for different cations appear as narrow peaks with few wavenumber widths.

4.1. Formation of ions by charge transfer from He⁺

The Poisson pressure dependences in Fig. 3 indicate that free $C_2H_2^+$ and $C_2H_3^+$ are mainly produced upon ionization of single embedded ethylene molecules. At small pickup pressures when doped droplets mostly contain single ethylene molecules, the dominant cationic products in the probe ionizer, such as in Fig. 1, are $C_2H_2^+$ and $C_2H_3^+$ with yield ratio of about 1:3. Electron impact ionization of free ethylene molecules yields $C_2H_4^+$, $C_2H_3^+$, $C_2H_2^+$, and C_2H^+ ions with the intensity in the ratio of $\sim 100:65:55:10.^{54}$ This is inconsistent with observations in helium droplets. Although the electron impact ionization cross section of ethylene is a factor of 10 larger than for helium atoms, the probability of ionizing one of the 7000 helium atoms of the droplet is about a factor of 700 larger than for ethylene molecule. Therefore, cations are likely produced in charge transfer reactions from He⁺ ions. Charge transfer from He⁺ to C_2H_4 in the gas phase produces $C_2H_4^+$, $C_2H_3^+$,

 $C_2H_2^+$, C_2H^+ , CH_3^+ and CH_2^+ ions with a yield ratio of ~ 7:5:64:13:2:12.⁵⁵ Although the reaction with He⁺ is consistent with the observed high yield of $C_2H_2^+$ in Fig. 2, it also predicts a small yield of $C_2H_3^+$ which is the dominant ion in Fig. 2. It is likely that the yields of ions produced in charge transfer in helium droplets differs from those in gas. In the droplets, He⁺ ions rapidly form He₃⁺ units, which may induce a different fragmentation pattern as compared with bare ions. Interaction with the helium environment may result in some relaxation of the highly excited ionic states from which the dissociation takes place. However, the study of these effects is beyond the scope of the present study. For now, we assume that $C_2H_2^+$, $C_2H_3^+$, $C_2H_4^+$ and CH_2^+ are the primary products of the ionization of single ethylene molecules in helium droplets in reactions (2-5).

$$C_2H_4 + He^+ \rightarrow C_2H_2^+ + H_2 + He$$
 (2)

$$C_2H_4 + He^+ \rightarrow C_2H_3^+ + H + He$$
 (3)

$$C_2H_4 + He^+ \rightarrow C_2H_4^+ + He$$
 (4)

$$C_2H_4 + He^+ \rightarrow CH_2^+ + CH_2 + He$$
 (5)

The infrared spectrum in Fig. 4 indicates that $C_2H_2^+$ and $C_2H_3^+$ and to smaller extent, $C_2H_4^+$ and CH_2^+ are the dominant embedded ions. The pickup pressure dependences show that $C_2H_2^+$ and $C_2H_3^+$ stem from single embedded ethylene molecules. This is consistent with our previous observation that ionization of single embedded CH_4 molecules produces a high yield of embedded CH_3^+ ions. The relative efficiency of producing free and embedded ions may be gleaned upon by the comparison of the QMS signal ion intensity as obtained without a laser and with a laser in measurements described in relation to Fig. 2 and Fig. 6, respectively. We will refer to these intensities as I_{probe} and I_{laser} , respectively. Both I_{probe} and I_{laser} can be expressed as integrals over time. I_{laser} is the integral over the signal duration of \sim 5 μ s in width. This time adds from the extraction time of the ions from the ion range of the probe ionizer of \sim 3 μ s as well the effect of the time constant of the pre-amplifier. We assume that the ions released from the droplets inside the laser beam waist along the axis of the ion range of \sim 1 cm length, see Fig. 1. Taking the velocity of the droplet beam of \sim 400 m/s, the flight time of the droplets through the ion range is \sim 25 μ s and was used for the integration to obtain I_{probe} . We obtain that for both dominant $C_2H_2^+$ and $C_2H_3^+$ ions, $I_{probe}/I_{laser} \approx 50$. For further comparison we note that I_{probe} is drawn upon ionization of the

entire helium droplet beam whose cross section is given by the 5 mm diameter aperture of the ion range. In comparison, I_{laser} stems from a laser beam waist of ~1 mm diameter as estimated from paper burns, i.e. a factor of ~25 smaller volume. The laser pulse energy dependence in Fig. 7 does not show any saturation, which indicates that the maximum laser pulsed energy used of ~4 mJ is insufficient for the release of ions from all droplets within the laser beam waist. In addition, the measurements of I_{laser} were performed at a fixed mass of the dominant bare ion products and did not include contribution from the clusters of ions with a few helium atoms, such as in Fig. 5. Therefore, we conclude that the electron impact ionization of the ethylene doped droplets with about 7000 helium atoms have comparable yield of free and embedded $C_2H_2^+$ and $C_2H_3^+$ ions. In fact, the yield of the embedded products may turn out to be dominant considering that I_{laser} considerably underestimates the amount of embedded ions.

It has long been observed that the electron impact ionization of helium droplets yields a series of He_N⁺ ions as well as ions that stem from the embedded molecules and clusters. 41, 42 The electron impact ionization of one of the helium atoms in the droplet is followed by charge transfer to the embedded molecule and dissociative ionization. Due to the larger ionization potential of helium (IP_{He}=24.6 eV) as compared with other molecules (IP_{ethylene}= 10.5 eV) the resulting energy release of about 14 eV is sufficient for the evaporation of the entire droplet. Penning ionization including He* (19.8 eV) metastable atoms which are also produced upon electron impact may constitute another ionization channel. Recall that 1 eV of energy is sufficient for thermal evaporation of ~1500 helium atoms from the droplet. Therefore, it was widely believed that droplets of few thousands of helium atoms are destroyed upon electron impact giving rise to predominantly free dopant ions and small He_N⁺ splitter ions. ^{42,56} Our results disagree with this conjecture and show a high yield of embedded ions. The precise mechanism for the mitigation of energy released upon charge transfer remains to be studied. It is feasible that a large portion of this energy is transferred to the translational energy of H, H₂ and CH₂ products that leave the droplet. Hydrogen atoms are known to repel helium atoms and H₂ molecules are weakly bound and are likely easily escaping the droplets. Small neutrals such as CH₂, C₂H₂ and C₂H₄ may also leave the droplet if they possess sufficient kinetic energy. Previously, it was observed that free alkyl radicals leave droplets upon photodissociation of embedded alkyl iodides such as CF₃I, C₂H₃I and CH₃I.⁵⁷

4.2. Formation of larger ions by ion molecule reactions

Larger ions containing three or four carbon atoms can be produced from primary ions via the following ion molecule reactions:⁵⁵

$$C_2H_2^+ + C_2H_4 \to C_2H_4^+ + C_2H_2$$
 (6)

$$C_2H_2^+ + C_2H_4 \rightarrow C_3H_3^+ + CH_3$$
 (7)

$$C_2H_2^+ + C_2H_4 \rightarrow C_4H_5^+ + H$$
 (8)

$$C_2H_3^+ + C_2H_4 \rightarrow C_2H_5^+ + C_2H_2$$
 (9)

$$C_2H_3^+ + C_2H_4 \rightarrow C_3H_3^+ + CH_4$$
 (10)

$$C_2H_3^+ + C_2H_4 \rightarrow C_4H_5^+ + H_2$$
 (11)

$$C_2H_4^+ + C_2H_4 \rightarrow C_3H_5^+ + CH_3$$
 (12)

$$C_2H_4^+ + C_2H_4 \rightarrow C_4H_7^+ + H$$
 (13)

The pressure dependence of the intensity of cations with three and four carbon atoms have a quadratic initial pressure rise and maxima around 6×10^{-6} mbar, consistent with their production in the bimolecular charge transfer reactions (6-13). Reactions (6-13) were identified in the gas phase at room temperature. It is unclear how the rate of these reactions would change at temperature of about 1 K. On the other hand, the ions will likely originate in some vibrationally or electronic excited states and may react before cooling. Good agreement of the yield of the free primary ions with Poisson probability for picking up a single ethylene molecule is apparent in Fig. 3. In addition, we did not observe any indication of the presence of unreacted cationic complexes with ethylene molecules in the infrared spectra in Fig. 4. In comparison, previous studies of the embedded molecules inevitably revealed additional bands due to small molecular clusters. These findings may indicate that the ion molecular reactions proceed to completion in helium droplets such that no unreactive complexes of primary ions with ethylene molecules remain. In addition to the bimolecular reactions above, $C_4H_7^+$ can also be produced in droplets via recombination reaction:

$$C_2H_3^+ + C_2H_4 \rightarrow C_4H_7^+$$
 (14)

The reaction schemes presented above explain the presence of all ions identified upon electron impact ionization, both free and embedded. Accordingly, CH_2^+ , $C_2H_2^+$, $C_2H_3^+$ and $C_2H_4^+$ are

produced upon charge transfer from He⁺ ions in reactions (2-5) and are the most abundant products. C₃H₃⁺, C₃H₅⁺, C₄H₅⁺ and C₄H₇⁺ are secondary ions with smaller abundance originated from the reaction of primary ions with ethylene molecules (6-14). Therefore, the composition of the embedded ions produced from some other precursors may be anticipated knowing the primary ions produced upon the electron impact ionization and reactions of primary ions with the precursors. The only notable exception from this scheme is C₂H₅⁺ which is expected to be produced by proton transfer in reaction (9). Free C₂H₅⁺ ions produce a strong peak in Fig. 2. On the other hand, the absence of the signal assigned to these ions in Fig. 4 indicates their retention by helium droplets is inefficient. The lack of protonated ethylene contrasts with our previous studies of ionization of water clusters in helium droplets ⁴⁶, where a strong spectrum from protonated water dimers (H₅O₂⁺) was observed. The origin of the inefficient production of embedded protonated hydrocarbons deserves further investigation. It is interesting that embedded C₂H₄⁺ comes from ionization of the dimers. It is feasible that ionization of single ethylene molecules leads to some highly excited electronic state which is ejected or whose relaxation indeed evaporates the entire droplet. Thus, production of C₂H₄⁺ by charge transfer from C₂H₂⁺ in reaction (6) may give the system an opportunity to get rid of excess energy by kicking off C₂H₂ molecules.

4.3. Free ions

Figure 6 shows that substantial fraction of free ions produced upon infrared laser excitation has one or few attached helium atoms. For CH_2^+ , the signals due to bare ions and ions containing a few helium atoms are comparable, whereas for $C_2H_2^+$ and $C_2H_4^+$ the peak due to bare ions is a factor of ~10 stronger. A similar effect was found by Drabbels *et al.*, for aniline ions released from helium droplets upon infrared excitation.³⁸ The binding energy of helium atoms to a molecular ion such as CH_3^+ is of the order of 100 - 200 cm⁻¹ for the most strongly bound helium atoms.⁵⁸ Our results are consistent with free ions released upon multiple sequential events of absorption of infrared quanta by cations followed by the transfer of the absorbed energy to the droplets and evaporation of helium atoms.⁴⁶ Absorption of one quantum of ~3000 cm⁻¹ radiation leads to thermal evaporation of about 600 helium atoms. Thus, the absorption of $n\approx10$ quanta is required for the thermal evaporation of the droplets used in this work. Upon absorption of the first n-1 quanta, the helium droplet size decreases such that it contains a few hundred atoms. The vibrational frequency of the molecules within a fraction of the wavenumber does not depend on the number

of helium atoms in droplets larger than \sim 500 atoms.⁵⁹ Upon absorption of the last n-th photon, the last few hundred helium atoms evaporate leaving bare cations or those having a few helium atoms attached, depending on the number of helium atoms in the droplet before the last absorption. Bare cations or those with a few helium atoms attached have their vibrational frequency shifted by few wavenumbers with respect to those in droplets. Therefore, they come out of the resonance with the laser infrared radiation and cannot be further excited. The resulting abundance of the ions with a few helium atoms attached may depend on several factors, such as binding strength of helium atoms with cations as well as the line width of the absorption and the amount of spectral shift induced by the helium matrix. Nevertheless, the appearance of ions with helium atoms attached indicates that the cations have internal temperature of about or less than 100 K. Therefore, the measurements could likely be expanded to complexes of ions with other species, such as $C_2H_2^+$ - H_2 , which presence is suggested in Fig. 5.

4.4. Spectroscopy and comparison with gas, matrix and tagging

	in gas	Tagged	in matrix	in He	Neutralized
					from Ref. ⁶⁰
$CH_{2}^{+}(v_{3})$	3131.37 ¹⁷			3159.6 ^{a)}	3190
$CH_3^+(v_3)$	3107.85 ¹⁸	3121.3		3128.1	3160.8
	Oka	+2He ²⁶			
$C_2H_2^+(v_3)$	3135.98 ¹⁹	3152.73		3140.0	3294.9 FR
		+Ar ⁶¹			3281.9 FR
$C_2H_3^+(v_6)$	3142.3 ²⁰	3146.3		3145.7	2901.9
bridged		+Ar ⁵¹			vinyl
$C_2H_4^+(v_{11})$	2978.7		3014.4 in Ne ³⁰	3007.0	2988.7
	from PES ⁵⁰		3028.7 in Ar ³¹		
$C_2H_4^+(v_9)$			3153.5 in Ar ³¹	3102.7	3105.5

a) The frequency of the dominant peak in the spectrum.

Table 1. C-H vibrational frequencies for cations obtained in gas, via tagging, in solid matrix and in helium droplets. The last column given the frequencies for the corresponding neutral species. All values and in units of wavenumbers.

Table 1 shows a comparison of the frequencies of the C-H bands in small carbocations studied in this work with previous measurements in gas phase, by tagging with rare gas (Rg) atoms and in solid matrices. It's seen that frequencies in helium are within about ± 20 cm⁻¹ and coincide with those in the gas phase when available. The gas phase absorption spectra of small cations listed in Table 1 were obtained in discharges, which could not be easily extended to larger ions due to small number densities. In some cases, the vibrational frequencies of cations were deduced from the high-resolution photoelectron spectra (PES), such as for $C_2H_4^{+.50}$ However, the PES has different selection rules and not all infrared active vibrations could be accessed. Tagging of cations by Rg atoms was used to obtain the spectra of numerous cations.^{22, 23, 62, 63} In this technique, the spectrum of a complex of a cation with a Rg atom is obtained which often has some extra bands which requires some additional efforts to interpret. The bands of the complexes typically have widths of the order of few tens of the wavenumbers, which often causes the spectral congestion of

different bands. Figure 9 shows a comparison of the spectrum of the $C_2H_3^+$ in helium droplets with that for the argon-tagged cations.⁵¹ It is seen that the spectrum in helium is a factor of ~10 narrower as compared with the tagged cations where the linewidth was ascribed to unresolved rotational structure of the complexes with internal temperature of ~100 K. The spectrum of the $C_2H_3^+$ in helium is represented by a single narrow line, which is consistent with the bridged C_{2v} non-classical structure in agreement with earlier works.^{20, 51}

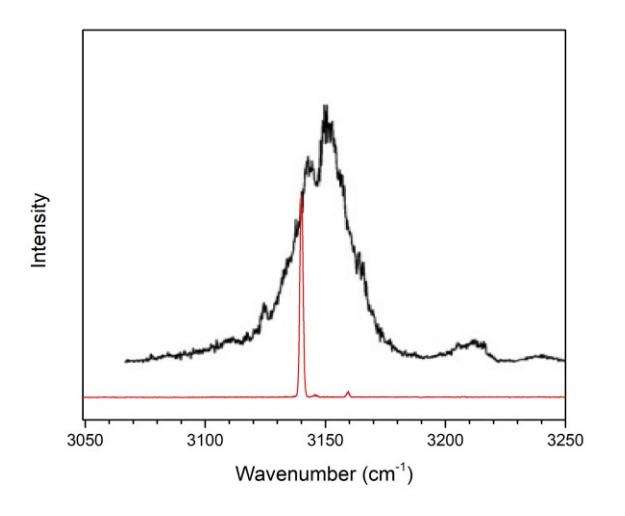


Figure 9. The comparison of the spectrum of $C_2H_3^+$ -Ar with the spectrum of $C_2H_3^+$ in helium droplets.

The vibrational frequencies of neutral molecules in solid matrices and liquid helium droplets are often shifted towards low frequencies due to larger solvation energy of the vibrationally excited species. $^{34-36}$ Table 1 shows that the studied cations in helium, except $C_2H_3^+$, experience a high frequency shift. This effect may be related to small transfer of the electron density from the surrounding helium atoms, as it was previously discussed in relation to CH_3^+ . 47 , 58 Overall the helium matrix shift is of the order or smaller than ± 20 cm $^{-1}$, which is comparable (or better) than the accuracy of quantum chemical calculations currently. Therefore, the measurement of the frequencies of cations in helium droplets could be compared with the results of quantum chemical calculations for free cations to determine structure.

4.5 Rotation of ions in helium droplets

We previously observed that the v_3 band of CH_3^+ in helium droplets has three prominent peaks that were assigned to partially resolved rotational structure of the K' \leftarrow K" sub-bands of the

perpendicular transition.⁴⁷ The K"=0 and K"=1 remain populated in helium droplets due to their different nuclear spin states which interconversion is slow in helium droplets. Similar result was previously observed for small symmetric molecules, such as SF₆, NH₃, CH₄ and C_2H_6 .⁶⁴⁻⁶⁷ Previous extensive studies of neutral species in helium droplets have shown that the spectra could be described by introducing effective rotational constants with values close to or up to a factor of about three smaller than for free molecules.³⁴⁻³⁷ In comparison, the effect was observed to be larger in CH₃⁺ and manifested dramatically different for rotation around the C₃ axis and perpendicular to it, where the rotational constants of free molecules of $A(I-\zeta)$ =4.05, B=9.27 decrease in helium to about 3.4 cm⁻¹ and <0.1 cm⁻¹, respectively. This unusually large disparity is explained by a strong and anisotropic interaction of CH₃⁺ with helium atoms. The interaction along the partially filled 2pz orbital of carbon atoms draws two helium atoms to the complex, making an effective He-CH₃⁺-He rotor. On the other hand, we concluded that other atoms in the first solvation shell of CH₃⁺ likely continue participating into the exchange with more distant helium atoms of the superfluid droplet.

Among the ions presented in Fig. 6, only the 3153.5 cm⁻¹ band of $C_2H_4^+$ shows the triplet (3100.3, 3105.3, 3110.4 cm⁻¹) which could be assigned to the rotational structure of the *b*-type v_9 band. The free $C_2H_4^+$ in the ground X $^2B_{3u}$ has an effective D_{2h} symmetry and has nuclear spin isomers. 68 $C_2H_4^+$ is nearly a symmetric top with A=4.77, B=0.93 and C=0.78 cm⁻¹. 69 The rotational constant A= 2.5 cm⁻¹ and band origin at 3102.7 cm⁻¹ can be obtained from Fig. 6. The value of the B and C constants could not be determined. Taking into account the width of the sub-bands of $\delta v \approx 1.5$ cm⁻¹ FWHM, which is very close to nominal laser linewidth of 1 cm⁻¹, we concluded that the B and C constants of $C_2H_4^+$ are small (<0.3 cm⁻¹) and could not be determined. This is in agreement with the absence of any rotational structure in the *a*-type v_{11} 3007 cm⁻¹ band which has $\delta v \approx 1$ cm⁻¹. These results show that the A constant for rotation over the C-C axis decreases in helium by about a factor of 2, whereas the decrease of the end over end rotational constant is probably much larger but could not be determined.

The free $C_2H_2^+$ ions have a $^2\Pi_u$ ground state with rotational constant of B=1.104 cm⁻¹ and spin-orbit interaction constant of A=-30.91 cm⁻¹.¹⁹ The rotational angular momentum N and the electron spin angular momentum S couple to make the total angular momentum J=N+S, and the spectrum consists of two series of F_1 and F_2 corresponding to J=N+1/2 and J=N-1/2. The Λ -doubling components have intensity ratio of 3:1 due to the nuclear spin of protons.¹⁹ It is likely

that in helium droplets the ions relax into the lowest spin orbit component as it was previously observed for NO molecules in helium droplets.⁷⁰ Therefore, at low temperature the spectrum should be represented by the Q(J=3/2) and R(J=3/2) which have splitting of about 5.3 cm⁻¹ in the gas phase.¹⁹ The band of $C_2H_2^+$ in Fig. 6 appears as a single peak with the width of 1.5 cm⁻¹ FWHM, which indicates that the rotational constant B in helium is much less than in free ions, but could not be determined in the present work.

Free CH_2^+ ion in the ground X 2A_1 state is close to linear with rotational constants $A=69.5~cm^{-1}$, $B=7.85~cm^{-1}$ and $C=6.92~cm^{-1}.^{71}$ The spectrum of CH_2^+ in helium droplets show two narrow ($\delta v \approx 1.3~cm^{-1}$) lines at 3146.8 and 3159.6 cm⁻¹ with intensity ratio of about 1:10. The splitting between the lines of 12.8 cm⁻¹ is rather close to the value of $B+C=14.8~cm^{-1}$ in the gas phase, which hints it may relate to the rotational structure of CH_2^+ in helium. The lowest levels of the para- and ortho- modifications of CH_2^+ should be 0_{00} and 1_{01} , neglecting electron spin, similar to that for water molecules. The a-type spectrum of CH_2^+ is close to that for a linear molecule and at low temperature should consist of three lines equivalent to the P(1), P(0) and P(1) lines of a linear rotor. Because only two lines were observed in helium droplets, the assignment could not be made. If the rotational structure is indeed responsible for the appearance of the two lines of P(1), the position of its band origin in Table 1 should be revised. Its current value corresponds to the frequency of the most intense line in the spectrum.

In the gas phase $C_2H_3^+$ is a nearly symmetric top with A=13.3 cm⁻¹, B=1.14 cm⁻¹ and C=1.05 cm⁻¹.²⁰ The fact that the a-type band of $C_2H_3^+$ in helium droplets appears as a single peak with $\delta v \approx 1.3$ cm⁻¹ FWHM was observed for in Fig. 6 likely indicates considerable drop of the constants B and C for the end over end rotation in helium. The discussion of the rotational spectra in this section assumes that the interconversion between the nuclear spin isomers of symmetric ions is inefficient in helium droplets. This assumption appears valid for CH_3^+ and $C_2H_4^+$, however its generality for other ions should be further evaluated. It is feasible that the relaxation of the nuclear spin in ions is faster than in neutrals due to magnetic moment induced by rotation of ions as well as due to magnetic moment of the electron angular momentum and electron spin, such as in the $^2\Pi$ state.

5. Conclusions

This work demonstrates that helium droplets are an open system, akin a test tube. It was well known that neutral precursors are easily captured by the droplets. Here we have shown that ionization of neutral species produces embedded splitter ions with a high yield. The light products such as hydrogen atoms and small molecules such as H₂, CH₂ etc. easily leave the droplets carrying away excess energy that contributes to stabilization of the cations inside. If two ethylene molecules are present, the primary ions originate by charge transfer from He⁺ ions which react with ethylene and produce secondary ions. These ions contain three to four carbon atoms that stabilize by shedding hydrogen atoms and H₂ molecules. Ions such as C₃H₃⁺, C₃H₅⁺, C₄H₅⁺, C₄H₇⁺ etc. have structural isomers interconversion between which was invoked in reactions of carbo-cations.⁵ It would be interesting to extend the infrared spectroscopic studies in helium droplets to study of the structure of larger cations. We expect that larger cations could be produced and studied upon application of the appropriate precursor molecules. The technique is especially useful for carbocations which could not be easily produced via other methods such as photoionizatoin³⁸ or electrosprav⁴⁰.

The vibrational spectra of the cations are obtained upon irradiation with resonant infrared laser radiation which causes the release of the cations from the droplets. The spectra are nearly background free and demonstrate a high signal to noise ratio of ~1000 for the strong bands and concomitant large dynamic range for the measurements. This experiment does not require double mass spectrometer and/or cryogenic traps that are often applied in the contemporary works with tagging. Infrared spectra of the cations in the CH-stretching range show narrow vibrational bands with a few wavenumbers in width, which is an order of magnitude less than previously obtained in solid matrices or in tagged complexes. Comparison with previous studies of some small free cations shows that the helium matrix introduces a shift of vibrational frequencies of about ±20 cm⁻¹ or less, which enables direct comparisons with the results of quantum chemical calculations for structure determination. This technique may be especially useful to determine the structure of some prototypical cations of organic molecules, and radicals as well as protonated species.

6. Acknowledgements

This work was supported by the National Science Foundation under Grant CHE-1664990.

7. Data Availability Statement

The data that support the findings of this study are available from the corresponding author upon reasonable request.

8. References

- ¹ N. Agmon, H. J. Bakker, R. K. Campen, R. H. Henchman, P. Pohl, S. Roke, M. Thämer, and A. Hassanali, "Protons and Hydroxide Ions in Aqueous Systems," Chem. Rev. **116**, 7642-7672 (2016).
- ² N. S. Shuman, D. E. Hunton, and A. A. Viggiano, "Ambient and Modified Atmospheric Ion Chemistry: From Top to Bottom," Chem. Rev. **115**, 4542-4570 (2015).
- ³ A. G. G. M. Tielens, *The Physics and Chemistry of the Interstellar Medium* (Cambridge University Press, Cambridge, 2005).
- ⁴ G. A. Olah, G. K. Surya Prakash, K. Wade, A. Molnar, and R. E. Williams, *Hypercarbon Chemistry* (John Wiley & Sons, Hoboken, New Jersey, 2011).
- ⁵ G. A. Olah, G. K. S. Prakash, A. Molnar, and J. Sommer, *Superacid Chemistry* (John Wiley & Sons, Hoboken, New Jersey, 2009).
- 6 R. F. Frey, and E. R. Davidson, "Potential energy surfaces of CH₄+," J. Chem. Phys. **88**, 1775-1785 (1988).
- ⁷ H. J. Wörner, R. van der Veen, and F. Merkt, "Jahn-Teller Effect in the Methane Cation: Rovibronic Structure and the Geometric Phase," Phys. Rev. Lett. **97**, 173003 (2006).
- ⁸ E. T. White, J. Tang, and T. Oka, "CH₅⁺: The infrared spectrum observed," Science **284**, 135-137 (1999).
- 9 O. Asvany, P. Kumar, B. Redlich, I. Hegemann, S. Schlemmer, and D. Marx, "Understanding the infrared spectrum of bare CH₅+," Science **309**, 1219-1222 (2005).
- ¹⁰ O. Asvany, K. M. T. Yamada, S. Brunken, A. Potapov, and S. Schlemmer, "Experimental ground-state combination differences of CH₅+," Science **347**, 1346-1349 (2015).
- 11 H.-U. Siehl, Chapter One The Conundrum of the (C_4H_7)⁺ Cation: Bicyclobutonium and Related Carbocations in *Adv. Phys. Org. Chem.*, edited by I. H. Williams, and N. H. Williams (Academic Press, 2018), pp. 1-47.
- ¹² G. A. Olah, V. P. Reddy, and G. K. S. Prakash, "Long-lived cyclopropylcarbinyl cations," Chem. Rev. **92**, 69-95 (1992).
- ¹³ G. A. Olah, G. K. Surya Prakash, and G. Rasul, "Ab Initio/GIAO-CCSD(T) Study of Structures, Energies, and 13C NMR Chemical Shifts of C4H7+ and C5H9+ Ions: Relative Stability and Dynamic Aspects of the Cyclopropylcarbinyl vs Bicyclobutonium Ions," J. Am. Chem. Soc. **130**, 9168-9172 (2008).
- ¹⁴ V. Buss, P. V. R. Schleyer, and L. C. Allen, The Electronic Structure and Stereochemistry of Simple Carbonium Ions in *Topics in Stereochemistry*, edited by N. L. Allinger, and E. L. Eliel (John Wilesy & Sons, 1973), pp. 253-293.
- ¹⁵ A. G. Császár, C. Fábri, and J. Sarka, "Quasistructural molecules," WIREs Computational Molecular Science **10**, e1432 (2020).

- ¹⁶ A. B. McCoy, "Diffusion Monte Carlo approaches for investigating the structure and vibrational spectra of fluxional systems," Int Rev Phys Chem **25**, 77-107 (2006).
- 17 M. Rosslein, C. M. Gabrys, M. F. Jagod, and T. Oka, "Detection of the Infrared-Spectrum of CH_2^+ ," J. Mol. Spectrosc. **153**, 738-740 (1992).
- ¹⁸ M. W. Crofton, M. F. Jagod, B. D. Rehfuss, W. A. Kreiner, and T. Oka, "Infrared-Spectroscopy of Carbo-Ions .III. v₃ Band of Methyl Cation CH₃+," J. Chem. Phys. **88**, 666-678 (1988).
- ¹⁹ M. F. Jagod, M. Rösslein, C. M. Gabrys, B. D. Rehfuss, F. Scappini, M. W. Crofton, and T. Oka, "Infrared spectroscopy of carbo-ions. VI. C–H stretching vibration of the acetylene ion $C_2H_2^+$ and isotopic species," J. Chem. Phys. **97**, 7111-7123 (1992).
- 20 C. M. Gabrys, D. Uy, M. F. Jagod, T. Oka, and T. Amano, "Infrared Spectroscopy of Carboions. 8. Hollow Cathode Spectroscopy of Protonated Acetylene, $C_2H_3^+$," J. Phys. Chem. **99**, 15611-15623 (1995).
- ²¹ J. Roithova, A. Gray, E. Andris, J. Jasik, and D. Gerlich, "Helium Tagging Infrared Photodissociation Spectroscopy of Reactive Ions," Acc. Chem. Res. **49**, 223-230 (2016).
- ²² M. A. Duncan, "Infrared Laser Spectroscopy of Mass-Selected Carbocations," J. Phys. Chem. A **116**, 11477-11491 (2012).
- ²³ E. J. Bieske, and O. Dopfer, "High-Resolution Spectroscopy of Cluster Ions," Chem. Rev. **100**, 3963-3998 (2000).
- 24 D. W. Boo, and Y. T. Lee, "Infrared spectroscopy of the molecular hydrogen solvated carbonium ions, CH+5(H2)n (n=1–6)," J. Chem. Phys. **103**, 520-530 (1995).
- 25 C. J. Johnson, A. B. Wolk, J. A. Fournier, E. N. Sullivan, G. H. Weddle, and M. A. Johnson, "Communication: He-tagged Vibrational Spectra of the SarGlyH⁺ and H⁺(H₂O)_{2,3} Ions: Quantifying Tag effects in Cryogenic Ion Vibrational Predissociation (CIVP) Spectroscopy," J. Chem. Phys. **140**, 221101 (2014).
- ²⁶ M. Topfer, P. C. Schmid, H. Kohguchi, K. M. T. Yamada, S. Schlemmer, and O. Asvany, "Infrared photodissociation of cold CH₃⁺-He₂ complexes," Mol. Phys. **117**, 1481-1485 (2019).
- ²⁷ O. Asvany, C. R. Markus, T. Salomon, P. C. Schmid, S. Banhatti, S. Brünken, F. Lipparini, J. Gauss, and S. Schlemmer, "High-resolution rovibrational spectroscopy of c-C₃H₂+: The ν_7 C–H antisymmetric stretching band," J. Mol. Struct. **1214**, 128023 (2020).
- ²⁸ M. Tsuge, C.-Y. Tseng, and Y.-P. Lee, "Spectroscopy of prospective interstellar ions and radicals isolated in para-hydrogen matrices," Phys. Chem. Chem. Phys. **20**, 5344-5358 (2018).
- ²⁹ M. E. Jacox, "The spectroscopy of molecular reaction intermediates trapped in the solid rare gases," Chem. Soc. Rev. **31**, 108-115 (2002).
- 30 M. E. Jacox, and W. E. Thompson, "The infrared spectra of $C_2H_4^+$ and C_2H_3 trapped in solid neon," J. Chem. Phys. **134**, 064321 (2011).
- ³¹S.-C. Chen, M.-C. Liu, T.-P. Huang, C.-H. Chin, and Y.-J. Wu, "Photodissociation and infrared spectra of ethylene cations in solid argon," Chem. Phys. Lett. **630**, 96-100 (2015).
- ³² M. E. Jacox, and W. E. Thompson, "The production and spectroscopy of molecular ions isolated in solid neon," Res. Chem. Intermed **12**, 33-56 (1989).
- ³³ R. M. P. Tanyag, C. F. Jones, C. Bernando, S. M. O. O'Connell, D. Verma, and A. F. Vilesov, Experiments with large superfluid helium droplets in *Cold chemistry: Molecular scattering and reactivity near absolute zero*, edited by O. Dulieu, and A. Osterwalder (Royal Society of Chemistry, Cambridge, 2017), pp. 401-455.

- ³⁴ J. P. Toennies, and A. F. Vilesov, "Superfluid Helium Droplets: A Uniquely Cold Nanomatrix for Molecules and Molecular Complexes," Angewandte Chemie-International Edition **43**, 2622-2648 (2004).
- ³⁵ M. Y. Choi, G. E. Douberly, T. M. Falconer, W. K. Lewis, C. M. Lindsay, J. M. Merritt, P. L. Stiles, and R. E. Miller, "Infrared Spectroscopy of Helium Nanodroplets: Novel Methods for Physics and Chemistry," Int Rev Phys Chem **25**, 15-75 (2006).
- ³⁶ D. Verma, R. M. P. Tanyag, S. M. O. O'Connell, and A. F. Vilesov, "Infrared Spectroscopy in Superfluid Helium Droplets," Advances in Physics-X **4**, 1553569 (2018).
- ³⁷ C. Callegari, and W. E. Ernst, Helium Droplets as Nanocryostats for Molecular Spectroscopy from the Vacuum Ultravoilet to the Microwave regime in *Handbook of High-resolution Spectroscopy*, edited by M. Quack, and F. Merkt (John Wiley & Sons, Ltd., 2011), pp. 1551-1594. ³⁸ S. Smolarek, N. B. Brauer, W. J. Buma, and M. Drabbels, "IR Spectroscopy of Molecular Ions by Nonthermal Ion Ejection from Helium Nanodroplets," J. Am. Chem. Soc. **132**, 14086-14091 (2010).
- ³⁹ F. Bierau, P. Kupser, G. Meijer, and G. von Helden, "Catching Proteins in Liquid Helium Droplets," Phys. Rev. Lett. **105**, 133402 (2010).
- ⁴⁰ A. I. González Flórez, D. S. Ahn, S. Gewinner, W. Schollkopf, and G. von Helden, "IR Spectroscopy of Protonated Leu-enkephalin and its 18-crown-6 Complex Embedded in Helium Droplets," Phys. Chem. Chem. Phys. **17**, 21902-21911 (2015).
- ⁴¹ M. Lewerenz, B. Schilling, and J. P. Toennies, "Successive capture and coagulation of atoms and molecules to small clusters in large liquid-helium clusters," J. Chem. Phys. **102**, 8191-8207 (1995).
- ⁴² A. Mauracher, O. Echt, A. M. Ellis, S. Yang, D. K. Bohme, J. Postler, A. Kaiser, S. Denifl, and P. Scheier, "Cold physics and chemistry: Collisions, ionization and reactions inside helium nanodroplets close to zero K," Physics Reports-Review Section of Physics Letters **751**, 1-90 (2018).
- ⁴³ M. Kuhn, M. Renzler, J. Postler, S. Ralser, S. Spieler, M. Simpson, H. Linnartz, A. G. G. M. Tielens, J. Cami, A. Mauracher, Y. Wang, M. Alcami, F. Martin, M. K. Beyer, R. Wester, A. Lindinger, and P. Scheier, "Atomically Resolved Phase Transition of Fullerene Cations Solvated in Helium Droplets," Nat.Comm. *7*, 13550 (2016).
- ⁴⁴ J. A. Davies, N. A. Besley, S. F. Yang, and A. M. Ellis, "Probing Elusive Cations: Infrared Spectroscopy of Protonated Acetic Acid," J. Phys. Chem. Lett. **10**, 2108-2112 (2019).
- 45 J. A. Davies, N. A. Besley, S. Yang, and A. M. Ellis, "Infrared spectroscopy of a small ion solvated by helium: OH stretching region of He_N-HOCO⁺," J. Chem. Phys. **151**, 194307 (2019).
- ⁴⁶ D. Verma, S. Erukala, and A. Vilesov, "Infrared Spectroscopy of Water and Zundel cations in Helium Nanodroplets," J. Phys. Chem. A **124**, 6207-6213 (2020).
- 47 S. Erukala, D. Verma, and A. Vilesov, "Rotation of CH₃+ Cations in Helium Droplets," J. Phys. Chem. Lett **12**, 5105-5109 (2021).
- ⁴⁸ D. Verma, and A. F. Vilesov, "Pulsed Helium Droplet Beams," Chem. Phys. Lett. **694**, 129-134 (2018).
- ⁴⁹ S. F. Yang, and A. M. Ellis, "Helium droplets: A chemistry perspective," Chem. Soc. Rev. **42**, 472-484 (2013).

- ⁵⁰ X. Xing, M.-K. Bahng, P. Wang, K.-C. Lau, S. J. Baek, and C. Y. Ng, "Rovibrationally selected and resolved state-to-state photoionization of ethylene using the infrared-vacuum ultraviolet pulsed field ionization-photoelectron method," J. Chem. Phys. **125**, 133304 (2006).
- ⁵¹G. E. Douberly, A. M. Ricks, B. W. Ticknor, W. C. McKee, P. v. R. Schleyer, and M. A. Duncan, "Infrared Photodissociation Spectroscopy of Protonated Acetylene and Its Clusters," J. Phys. Chem. A **112**, 1897-1906 (2008).
- ⁵² H. M. Wang, C. F. Neese, C. P. Morong, M. Kleshcheva, and T. Oka, "High-Resolution Near-Infrared Spectroscopy of CH₂⁺ and Its Deuterated Isotopologues," J. Phys. Chem. A **117**, 9908-9918 (2013).
- ⁵³ L. Tiefenthaler, J. Ameixa, P. Martini, S. Albertini, L. Ballauf, M. Zankl, M. Goulart, F. Laimer, K. v. Haeften, F. Zappa, and P. Scheier, "An intense source for cold cluster ions of a specific composition," Rev. Sci. Intrum. **91**, 033315 (2020).
- ⁵⁴ W. E. Wallace, Mass Spectra in *NIST Chemistry WebBook, NIST Standard Reference Database Number 69*, edited by P. J. Linstorm, and W. G. MallardNational Institute of Standards and Technology, Gaithersburg MD, 20899.
- ⁵⁵ V. G. Anicich, "An index of the literature for biomolecular gas phase cation-molecule reaction kinetics," in *JPL publication-03-19* (JPL publication-03-19, U.S., 2003).
- ⁵⁶ S. Albertini, E. Gruber, F. Zappa, S. Krasnokutski, F. Laimer, and P. Scheier, "Chemistry and physics of dopants embedded in helium droplets," Mass Spectrom. Rev. (2021).
- ⁵⁷ A. Braun, and M. Drabbels, "Photodissociation of alkyl iodides in helium nanodroplets. I. Kinetic energy transfer," J. Chem. Phys. **127**, 114303 (2007).
- ⁵⁸ O. Dopfer, and D. Luckhaus, "Rovibrational calculations for CH₃⁺−Rg (Rg=He,Ne): The prototype disk-and-ball dimer," J. Chem. Phys. **116**, 1012-1021 (2002).
- ⁵⁹ M. Hartmann, N. Portner, B. Sartakov, J. P. Toennies, and A. F. Vilesov, "High resolution infrared spectroscopy of single SF₆ molecules in helium droplets. I. Size effects in ⁴He droplets," J. Chem. Phys. **110**, 5109-5123 (1999).
- ⁶⁰ W. E. Wallace, Infrared Spectra in *NIST Chemistry WebBook, NIST Standard Reference Database Number 69*, edited by P. J. Linstorm, and W. G. MallardNational Institute of Standards and Technology, Gaithersburg MD, 20899.
- ⁶¹ O. Dopfer, R. V. Olkhov, M. Mladenović, and P. Botschwina, "Intermolecular interaction in an open-shell π -bound cationic complex: IR spectrum and coupled cluster calculations for C₂H₂⁺-Ar," J. Chem. Phys. **121**, 1744-1753 (2004).
- 62 L. I. Yeh, M. Okumura, J. D. Myers, J. M. Price, and Y. T. Lee, "Vibrational Spectroscopy of the Hydrated Hydronium Cluster Ions H₃O⁺.(H₂O)_n (n = 1, 2, 3)," J. Chem. Phys. **91**, 7319-7330 (1989).
- ⁶³ P. Ayotte, C. G. Bailey, J. Kim, and M. A. Johnson, "Vibrational predissociation spectroscopy of the $(H_2O)_6$ -·Ar_n, n≥6, clusters," J. Chem. Phys. **108**, 444-449 (1998).
- 64 M. Hartmann, R. E. Miller, J. P. Toennies, and A. Vilesov, "Rotationally resolved spectroscopy of SF₆ in liquid-helium clusters A molecular probe of cluster temperature," Phys. Rev. Lett. **75**, 1566-1569 (1995).
- 65 M. N. Slipchenko, and A. F. Vilesov, "Spectra of NH $_3$ in He droplets in the 3 μ m range," Chem. Phys. Lett. **412**, 176-183 (2005).
- ⁶⁶ H. Hoshina, D. Skvortsov, B. G. Sartakov, and A. F. Vilesov, "Rotation of methane and silane molecules in He droplets," J. Chem. Phys. **132**, 074302 (2010).

- 67 L. F. Gomez, R. Sliter, D. Skvortsov, H. Hoshina, G. E. Douberly, and A. F. Vilesov, "Infrared Spectra in the 3 μ m Region of Ethane and Ethane Clusters in Helium Droplets," J. Phys. Chem. A **117**, 13648-13653 (2013).
- ⁶⁸ C. M. Lindsay, and R. E. Miller, "Rotational and vibrational dynamics of ethylene in helium nanodroplets," J. Chem. Phys. **122**, 104306 (2005).
- ⁶⁹ X. Xing, B. Reed, M.-K. Bahng, and C. Y. Ng, "Infrared–Vacuum Ultraviolet Pulsed Field Ionization-Photoelectron Study of C₂H₄⁺ Using a High-Resolution Infrared Laser," J. Phys. Chem. A **112**, 2572-2578 (2008).
- ⁷⁰ H. Hoshina, M. Slipchenko, K. Prozument, D. Verma, M. W. Schmidt, J. Ivanic, and A. F. Vilesov, "Infrared spectroscopy and structure of (NO)_n clusters," J. Phys. Chem. A **120**, 527-534 (2016).
- 71 S. Willitsch, and F. Merkt, "Characterization of the \tilde{X}^2A_1 (0,0,0) ground vibronic state of CH₂⁺ by pulsed-field-ionization zero-kinetic-energy photoelectron spectroscopy," J. Chem. Phys. **118**, 2235-2241 (2003).
- 72 K. E. Kuyanov, M. N. Slipchenko, and A. F. Vilesov, "Spectra of the v_1 and v_3 Bands of Water Molecules in Helium Droplets," Chem. Phys. Lett. **427**, 5-9 (2006).